2019-05-01

Investigating the filtration behavior of metal fiber felt using CFD-DEM simulation

Liu, X

10.1080/19942060.2019.1608306
Engineering Applications of Computational Fluid Mechanics
Taylor & Francis Group

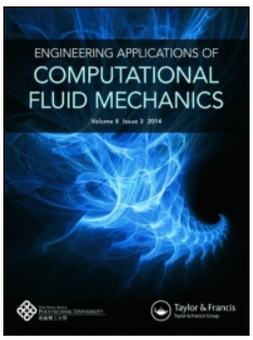

Engineering Applications of Computational Fluid Mechanics

ISSN: 1994-2060 (Print) 1997-003X (Online) Journal homepage: https://www.tandfonline.com/loi/tcfm20

Investigating the filtration behavior of metal fiber felt using CFD-DEM simulation

Xuedong Liu, Xinyue Ding, Cheng Chen, Rongrong An, Wenyuan Guo, Wei Zhang, Haijuan Nan & Yi Wang

To cite this article: Xuedong Liu, Xinyue Ding, Cheng Chen, Rongrong An, Wenyuan Guo, Wei Zhang, Haijuan Nan & Yi Wang (2019) Investigating the filtration behavior of metal fiber felt using CFD-DEM simulation, Engineering Applications of Computational Fluid Mechanics, 13:1, 426-437, DOI: 10.1080/19942060.2019.1608306

To link to this article: https://doi.org/10.1080/19942060.2019.1608306

Published online: 01 May 2019.

ENGINEERING APPLICATIONS OF COMPUTATIONAL FLUID MECHANICS
2019, VOL. 13, NO. 1, 426–437
https://doi.org/10.1080/19942060.2019.1608306

Taylor & Francis
Taylor & Francis Group

REVIEW ARTICLE

Investigating the filtration behavior of metal fiber felt using CFD-DEM simulation

Xuedong Liu[a,b], Xinyue Ding[a,b], Cheng Chen[a,b], Rongrong An[a,b], Wenyuan Guo[c], Wei Zhang[c], Haijuan Nan[d] and Yi Wang[e]

[a]School of Mechanical Engineering, Changzhou University, Changzhou, People's Republic of China; [b]Jiangsu Key Laboratory of Green Process Equipment of Changzhou University, Changzhou, People's Republic of China; [c]Sinopec Ningbo Engineering Co., Ltd, Ningbo, People's Republic of China; [d]West Baode Technologies Co., Ltd, Xi'an, People's Republic of China; [e]School of Business, Plymouth University, Plymouth, UK

ABSTRACT

This paper studies the dynamic filtration behavior of coal particles in metal fiber felt, by developing a three-dimensional model based on microstructure and arrangement mode of metal fiber felt identified by scanning electron microscope. Discrete element method (DEM) is coupled with Computational fluid dynamics (CFD) to simulate filtration of coal particles in metal fiber felt. The simulation mainly studies the moving trail and deposition characteristics of spherical coal particles. The results demonstrated that coal particles can bypass the metal fibers and enter the inside of the metal fiber felt through mesh channels. The moving trail of coal particles is similar to a broken line. It is also shown that most coal particles are trapped due to the deep filtration of metal fiber felt and the distribution pattern of them is inhomogeneous. The number of particles trapped by metal fiber felt is reduced in the direction of thickness. It is found that coal particles can be trapped not only by randomly arranged metal fibers, but also by coal particles deposited previously. Finally, the kinetic energy loss of coal particles mainly occurs in the initial stage when particles pass through metal fiber felt. And the velocity of coal particles inside metal fiber felt is maintained at 0.15–0.25 m/s.

Highlights

- A more realistic three-dimensional model was reconstructed according to scanning electron microscope pictures.
- The particle trajectory, deposition mode of particle groups and speed change of particles were investigated using CFD–DEM in the paper.
- The simulation method was validated by the experiment.

ARTICLE HISTORY
Received 13 November 2018
Accepted 12 April 2019

KEYWORDS
metal fiber felt; filtration; numerical simulation; CFD-DEM; particle

1. Introduction

With the process of urbanization and industrialization, the consumption of coal, oil and other non-renewable energy is increasing rapidly. Because of this, air pollution is getting worse and worse, especially PM 2.5, which would threaten people's health seriously. Pulverized coal particles produced by combustion is an important source of air pollution (Cai, Zhang, & Bao, 2018; Shi et al., 2018). Metal fiber felt has been widely used in removing fine particles in the air due to its excellent filtration performance (Mao et al., 2017; Nakamura, Suda, & Matsumoto, 2018; Tian, Qi, Su, Zhou, & Jing, 2016). Besides, it has an ideal uniform pore size distribution and excellent permeability. What's more, metal fiber felt has the characteristics of high temperature resistance, corrosion resistance, good thermal stability, high filtration efficiency and long service life. It is resistant to charring, burning bag at high temperature and particle leakage caused by long-term use of filter bag in filtration process, which can effectively reduce environmental pollution, services breakdown and instability of the equipment (Dong, 2016). So it is important to study the filtration characteristics of metal fiber felt to improve the filtration efficiency and prolong the service life. As computational capabilities are improved greatly, it is possible to predict the filtration performance of it in advance (Liu, Xu, & Liu, 2016; Mou, He, Zhao, & Chau, 2017; Ramezanizadeh, Nazari, Ahmadi, & Chau, 2019; Xu, Liu, & Pang, 2016).

Previous researchers have employed a variety of simulation methods to study the filtration process of fiber felt. Among this, computational fluid dynamics (CFD) is considered as a convenient and effective method to

CONTACT Xuedong Liu xdliu_65@126.com

simulate it (Sun et al., 2017; Wu, Lin, Hwang, Cheng, & Tung, 2018; Zhuang, Guo, Dai, & Xu, 2017). Kaya et al. (2014) used CFD simulation to analyze the influence of shear stress distribution and pressure loss on hollow fiber membrane. They established two computational models with different inlet and outlet, which were normal and tangential inlet and outlet respectively. Results were that tangential inlet and outlet enabled rotational flow, which could reduce plugging in membrane. In addition, Li, Shen, and Li (2016) employed a DPM model to study the filtration process. They found that the filtration efficiency was increased with the larger face velocity. Buetehorn et al. (2011) established a geometry model with computer tomography to study the influence of fiber arrangement on aeration efficiency. Results showed that the flow velocity and turbulent viscosity were greatly affected by the arrangement of fibers. Besides, a CFD porous media model was adopted by Ma et al. (2019) to simulate the effect of fiber distance on fiber-fiber interaction. They found that if the diameter of fiber was larger than fiber distance, the fiber-fiber interaction among fibers became important because of 'permeate competition'.

But these studies didn't consider the impact of particle deposition on filtration process, they were only fitted for the initial period of filtration. In order to study the real situation of filtration process, scholars at home and abroad have done a lot of research (Dong, Li, Shang, & Li, 2019; Saleh & Vahedi Tafreshi, 2015; Saleh, Hosseini, Vahedi Tafreshi, & Pourdeyhimi, 2013). For example, Dong et al. (2019) studied the process of particle deposition on fibers dynamically. They found that particles uniformly deposited on single fiber and were formed into small agglomerations at the initial process of deposition. Saleh et al. (2013) combined C++ subroutines with ANSYS CFD code to simulate the pressure and filtration efficiency in the case of particle loading. Besides, they compared the 1-D macroscale models with 3-D microscale simulation methods. And results showed that 3-D microscale simulation methods had a brighter future because of the high-speed development of computers. Hosseini and Vahedi Tafreshi (2012) used ANSYS-Fluent CFD code to simulate the collection efficiency and pressure drop of a single fiber. Results were that when the quality of particles remained constant, the coefficient decreased with the increase of particle diameter. Additionally, fiber drag force increased exponentially with the increase of deposition quality.

However, all of the above simulations were based on Lagrangian method. They only considered the interaction between particles and fluid, but ignored the forces of particle-fiber and particle-particle. Discrete element method (DEM) was initially proposed by Cundall and Strack (1979) to solve the issue. At present, the application of DEM in industry is gradually mature. JKR Cohesion model was adopted by Yang, Li, and Yao (2013) to study the sticking process of particles deposited on a single fiber, which was verified by the experiment of a single fiber. Dong, Zou, Yang, Yu, and Roach (2009) used DEM to study the growth of cake formation during the filtration process. Furthermore, considering that both CFD and DEM had their own advantages, researchers combined them together to study the two-phase flow under different conditions (Liu, Su, Qian, Cui, & Liu, 2018; Ma, Wei, Pei, Zhu, & Xu, 2018; Mahmoodi, Hosseini, & Ahmadi, 2018). Riefler, Ulrich, Morshäuser, and Fritsching (2018) studied particle penetration in fiber filters by using coupled DEM–CFD simulation. According to the study, they found most particles were deposited in the front part of the fiber filters. Besides, the number of particles that can pass through the fiber declined due to the particles deposited previously. In order to study the performance of filters, Yue, Zhang, and Zhai (2016) also applied CFD-DEM to analyze pressure drop and filtration efficiency in the simulation and results were validated by the semi-analytical models. Qian, Huang, Zhu, and Lu (2013) established a three-dimensional mathematical model based on SEM to study particle deposition and aggregation characteristics in filtration process. Besides, the influence of structural parameter on filtration process was also considered in the simulation. Qian, Huang, Lu, and Han (2014) further used CFD-DEM to simulate the dust-loading of particles during the filtration process in mimic structure.

This paper analyzes the filtration process of particles in metal fiber felt from a microscopic point of view. A three-dimensional model was reconstructed to simulate spherical particles in filtration process by computational fluid dynamics (CFD) and discrete element method (DEM). In the previous studies, the 3-D geometric model that researchers established could be divided into two types. One was a single fiber and the other was the mimic structure of the fibrous media. The research of a single fiber could simulate the relationship between particles and fibers more clearly. But it couldn't simulate the whole state of the fiber felt. Besides, the mimic structure was used by researchers to study the pressure drop and filtration efficiency of fibrous media. They keep the porosity of the model consistent with that of the actual material. But they didn't take the thickness of the actual material into consideration (Qian et al., 2013; Qian et al., 2014; Yue et al., 2016). In this article, the thickness of the model with 47 layers is 0.496 mm, which is almost consistent with the actual material. The study aims to analyze the particle trajectory, the deposition mode of particle groups and the speed change of particles during the whole process

of filtration, which provides a basis for improving the filtration efficiency of metal fiber felt.

2. Working principles

2.1. Equations governing gas phase

In CFD-DEM simulation, gas is considered as continuous phase. Its motion is controlled by the Navier-Stokes equation. So its continuity and momentum conservation equations are as follows (Blais, Bertrand, Fradette, & Bertrand, 2017)

$$\frac{\partial}{\partial t}(\varepsilon_g \rho_g) + \nabla \cdot (\varepsilon_g \rho_g \boldsymbol{u}_g) = 0 \tag{1}$$

$$\frac{\partial}{\partial t}(\varepsilon_g \rho_g \boldsymbol{u}_g) + \nabla \cdot (\varepsilon_g \rho_g \boldsymbol{u}_g \boldsymbol{u}_g) = -\varepsilon_g \nabla p + \nabla \cdot (\varepsilon_g \boldsymbol{\tau}_g) + \varepsilon_g \rho_g \mathbf{g} - \boldsymbol{S} \tag{2}$$

where ρ_g is the gas density, ε_g is gas porosity, p is the gas pressure, $\boldsymbol{u}_g$ is the gas velocity, $\boldsymbol{\tau}_g$ is viscous stress tensor, $\mathbf{g}$ is gravitational acceleration, and $\boldsymbol{S}$ is the momentum exchange between gas and solid.

2.2. Equations governing particle phase

The discrete element method is a numerical method suitable for solving the problem of discontinuous medium mechanics. Each particle is modeled as a unit, and the position and velocity of each particle are tracked. When particles move in the flow field, they are subjected to three external forces, including force between particles and fluid, the collision force between particles and particles or the wall. Besides, particle motion follows Newton's second law, and its governing equations consist of translational and rotational parts. The equation of motion is as follows (Wu, Gui, Yang, Tu, & Jiang, 2017)

$$m_i \frac{\mathrm{d}\boldsymbol{v}_i}{\mathrm{d}t} = m_i \mathbf{g} + \sum_{j=1}^{n} (\boldsymbol{F}_{n,ij} + \boldsymbol{F}_{t,ij}) + \boldsymbol{F}_{f,i} \tag{3}$$

$$I_i \frac{\mathrm{d}\omega_i}{\mathrm{d}_t} = \sum_{j=1}^{n} (\boldsymbol{R}_i \times \boldsymbol{F}_{t,ij}) + \sum_{j=1}^{n} \boldsymbol{M}_{r,ij} \tag{4}$$

where m_i is the particle mass, I_i is the inertia moment, $\boldsymbol{v}_i$ is the translational velocity, ω_i is the angular velocity, $m_i\mathbf{g}$ is the particle gravity, $\boldsymbol{F}_{n,ij}$ is the normal contact force between particles, $\boldsymbol{F}_{t,ij}$ is the tangential contact force between particles, $\boldsymbol{F}_{f,i}$ is the particle-fluid interaction force, $\mathbf{R}_i$ is the distance vector from particle centroid to contact point between particles and $\boldsymbol{M}_{r,ij}$ is the rolling friction torque.

Considering the multiple and long-time collision, a more realistic Hertz–Mindlin non-slip soft-sphere contact model is adopted. The external force and external torque of particles are as follows (Li & Ji, 2013)

$$\boldsymbol{F}_{n,ij} = k_n \delta \boldsymbol{n}_{ij} - \gamma_n \boldsymbol{V}_{n,ij} \tag{5}$$

$$\boldsymbol{F}_{t,ij} = k_t \delta \boldsymbol{t}_{ij} - \gamma_t \boldsymbol{V}_{t,ij} \tag{6}$$

$$\boldsymbol{M}_{r,ij} = -\frac{\omega_{ij}}{|\omega_{ij}|} \mu_r R_i F_{n,ij} \tag{7}$$

where $\boldsymbol{V}_{n,ij}$ and $\boldsymbol{V}_{t,ij}$ are relative velocity, $\delta \boldsymbol{n}_{ij}$ and $\delta \boldsymbol{t}_{ij}$ are deformations in normal and tangential directions, k_n and k_t are elastic coefficients, γ_n and γ_t are viscous damping coefficients and μ_r is the rolling friction coefficient. The elastic and viscous damping coefficients can be determined by the following formula

$$k_n = \frac{4}{3} E^* \sqrt{R^* \delta \boldsymbol{n}_{ij}} \tag{8}$$

$$k_t = 8 G^* \sqrt{R^* \delta \boldsymbol{n}_{ij}} \tag{9}$$

$$\gamma_n = -2\sqrt{\frac{5}{6}} \psi \sqrt{\frac{3}{2} k_n m^*} \tag{10}$$

$$\gamma_t = -2\sqrt{\frac{5}{6}} \psi \sqrt{k_t m^*} \tag{11}$$

where ψ is the damping coefficient, E^* is the Young's modulus, G^* is the shear modulus, R^* is the contact radius, and m^* is the equivalent mass, which are computed as

$$\frac{1}{m^*} = \frac{1}{m_i} + \frac{1}{m_j} \tag{12}$$

$$\frac{1}{R^*} = \frac{1}{R_i} + \frac{1}{R_j} \tag{13}$$

$$\frac{1}{E^*} = \frac{1 - \nu_i^2}{E_i} + \frac{1 - \nu_j^2}{E_j} \tag{14}$$

$$\frac{1}{G^*} = \frac{2(2 - \nu_i)(1 + \nu_i)}{E_i} + \frac{2(2 - \nu_j)(1 + \nu_j)}{E_j} \tag{15}$$

where ν is the Poisson ratio of the particle material. Besides, the damping coefficient is given by

$$\psi = \frac{\ln(e)}{\sqrt{\pi^2 + \ln^2(e)}} \tag{16}$$

where e is the restitution coefficient.

2.3. Gas-solid coupling sub model

2.3.1. Coupling algorithm of gas-solid phases

In coupled calculation, the gas-solid interaction force of a single particle is calculated firstly in each time step. And the gas-solid interaction force of gas phase in the grid can be obtained by summing up the gas-solid interaction force of particles in fluid calculation grid.

The gas-solid interaction force is formed by the interaction between particles and surrounding gas, which mainly include drag force, buoyancy, pressure gradient force, additional mass force, Basset force, Saffman force, Magnus force and so on. In order to simplify the calculation, only the effect of drag force is considered in this paper. Therefore, the equation of force acting on particles is as follows (Qian et al., 2014)

$$S = \frac{1}{\Delta V}\sum_{i=1}^{n} \boldsymbol{F}_{drag,i} \tag{17}$$

where ΔV is the volume of control body, and n is the number of particles in it.

2.3.2. Drag force model

When particles move with the surrounding fluid together, drag force exists between them due to the velocity difference. Among them, the one with higher velocity will drag the other one, while the one with lower velocity will hinder the movement of the other phase. Besides, drag force is proportional to the velocity difference between particles and fluid. The drag force $\boldsymbol{F}_{drag,i}$ is computed as (Gao, Li, Sarkar, Lu, & Rogers, 2018)

$$\boldsymbol{F}_{drag,i} = \frac{V_i\beta}{1-\varepsilon_g}(\boldsymbol{u}_g - \boldsymbol{v}_p) \tag{18}$$

where $\boldsymbol{v}_p$ is the velocity of particle in the current grid, V_i is the particle volume and β is the interphase momentum exchange coefficient. β is given as

$$\beta = \begin{cases} \frac{3}{4}C_d\frac{\rho_g\varepsilon_g(1-\varepsilon_g)|\boldsymbol{u}_g-\boldsymbol{v}_p|}{d_p}\varepsilon_g^{-2.65}\varepsilon_g \geq 0.8 \\ \frac{150(1-\varepsilon_g)^2\mu_g}{\varepsilon_g d_p^2} + \frac{1.75\rho_g(1-\varepsilon_g)|\boldsymbol{u}_g-\boldsymbol{v}_p|}{d_p}\varepsilon_g < 0.8 \end{cases} \tag{19}$$

$$C_d = \begin{cases} \frac{24}{Re_p}(1 + 0.15Re_p^{0.687})Re_p < 1000 \\ 0.44Re_p \geq 1000 \end{cases} \tag{20}$$

where d_p is the diameter of particle, C_d is the drag coefficient of a single particle, Re_p is the Reynolds number, and μ_g is the dynamic viscosity of fluid.

3. Models and CFD-DEM simulation

3.1. Fiber felt model

The metal fiber felt, as shown in Figure 1(a), is provided by West BaoDe Technologies Co., Ltd. It is made of 06Cr17Ni12Mo2, with the thickness of 0.5 mm and porosity of 80% ± 10%. Scanning electron microscope is used to observe the microstructure of the metal fiber felt and distribution of metal fibers. According to scanning results, the filter felt model can be effectively established. The results of the scanning electron microscope,

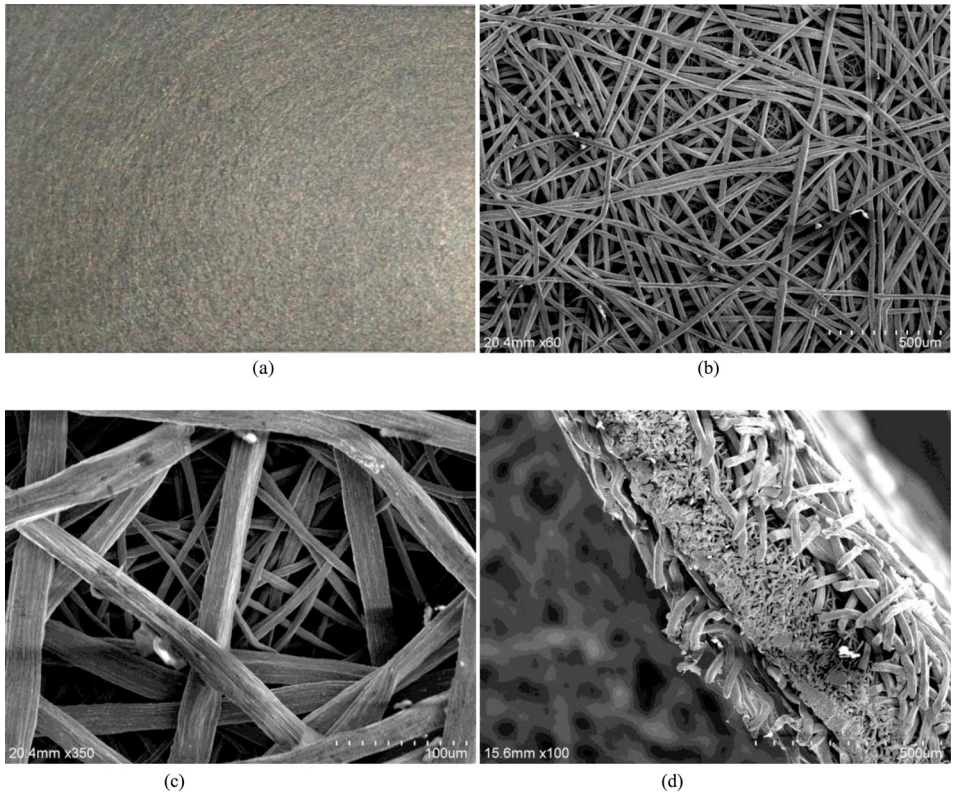

(a) (b) (c) (d)

Figure 1. SEM images of metal fiber felt.

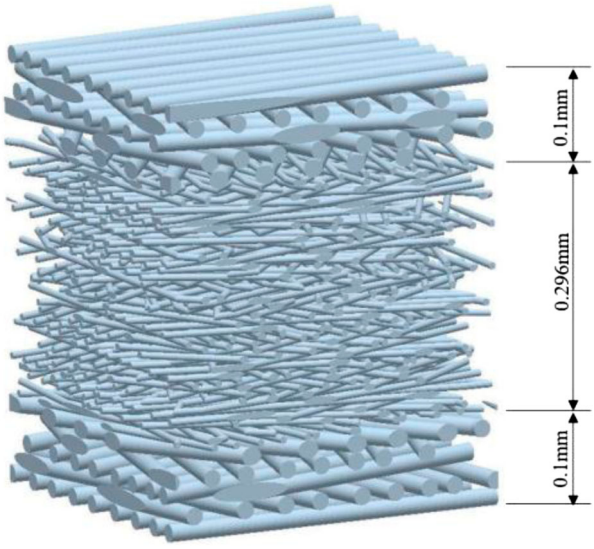

Figure 2. Fiber felt model.

as shown in Figure 1(b–d), illustrate that the metal fiber felt is similar to a 'sandwich' structure. Both the upper and lower sides are made of metal fibers with a diameter of 20 μm and the middle area is metal fiber with the diameter of 8 μm approximately. Multilayer metal fibers are processed by compression molding after weaving. There is no obvious direction of metal fiber arrangement. And the mesh channels formed by staggered fibers are of different sizes and no fixed shapes.

According to the results obtained by scanning electron microscope, Pro/Engineer 5 is used to simulate the production process of metal fiber felt, as shown in Figure 2. The metal fiber felt is made up of three regions. And the outside two regions are randomly arranged with cylindrical metal fibers of 20 μm in diameter, each of which is stacked with 5 layers. And thickness of the two regions is 0.1 mm, respectively. The middle region has 37 layers, consisting of cylindrical metal fibers with the diameter of 8 μm, whose thickness is 0.296 mm. So the total thickness of this model is 0.496 mm, which is basically consistent with the thickness of the actual metal fiber felt. In order to further verify the conformity between metal fiber felt model and the actual object, the porosity of metal fiber felt model was calculated to be 74.8%. It is consistent with that of the metal fiber felt factory report, which is 80% ± 10%.

3.2. Simulation conditions

The numerical simulation model of particle filtration is shown in Figure 3. The air inlet is on the left side, and particles are generated at position shown in the figure. Middle position is placed with the metal fiber felt model established above. Particles move from left to right gradually with the direction of air flow, and enter the internal area of metal fiber felt.

In the CFD-DEM coupling simulation, the inlet and outlet are set to be velocity-inlet and pressure outlet respectively. To ensure the steady airflow in the filtration process, inlet and outlet are set about 0.35 mm away from the felt. Meanwhile the computational domain is $0.4 \times 0.4 \times 1.2\ mm^3$ with the fiber felt thickness of 0.496 mm, which is big enough to make the filtration process independent of the computational domain size. Besides, the fibers are set to be wall in Fluent and other parts of the computational domain are set to be symmetry boundary conditions. In DEM, the interaction between particles and the surface of fibers is set to be no-slip boundary conditions. Lastly, the periodic boundary is applied in the computational domain. It is used to set the state of particles after they leave the computational domain. Due to this, particles that have left the computational domain will re-enter the computational domain from the opposite direction immediately.

Specifically, the velocity inlet is 1 m/s with the density and viscosity values of $1.185\ kg/m^3$ and 1.834×10^{-5} Pa s.

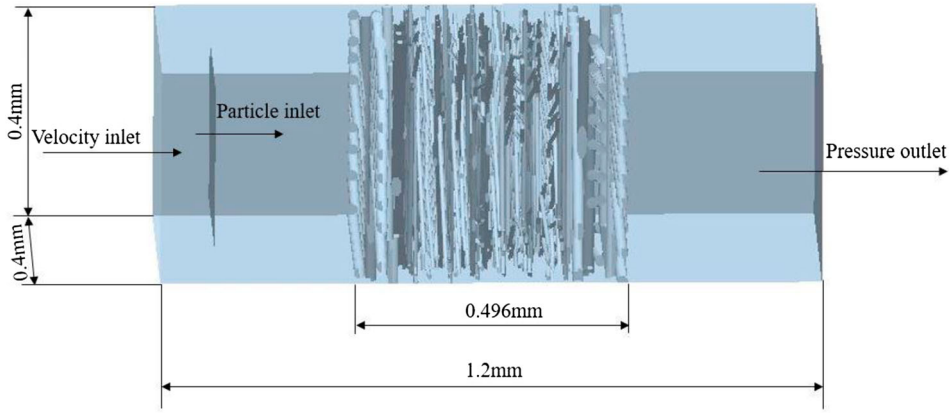

Figure 3. Particle filtration model.

The particle phase is set by EDEM 2.7. 1000 spherical coal particles are generated with particle diameter of 10 μm and particle density of 1400 kg/m^3. The material of metal fiber filter model is selected as stainless steel. Particles in this simulation are of consistent physical properties. Values of main parameter settings are shown in Table 1.

3.3. Computational grids

As the fiber in the model is arranged randomly and irregularly, it is difficult to generate hexahedral meshes relatively. Thus, unstructured meshes are employed in this model by using ICEM CFD. In the model, the diameter of fiber is much smaller than size of the inlet, so they are set to be different max grid sizes. The max grid size of the fiber is 0.008 mm, and the other parts of the model are set to be 0.04 mm. After calculation, the number of total elements in the model is 2311802. And the mesh of the model is shown in Figure 4.

To check the grid-independence, grids with different number of elements are generated. The first one is above, whose total elements are 2311802. And the following two are with elements of 3230385 and 4780104. The inlet velocity is 1 m/s and the diameter of particle is 10 μm. Pressure drop in filtration process is monitored in the simulation, which is shown in Figure 5. It shows that pressure drop tended to be stable with the increase of mesh density. And it proves that results are independent of the mesh density. Therefore, the mesh with elements of 2311802 is chosen for the simulation.

Table 1. Key parameter settings in the simulation.

Parameters	Particle	Fiber
Density/kg m^{-3}	1400	7900
Poisson's ratio	0.35	0.3
Shear modulus/Pa	1.3×10^9	7×10^{10}
Parameters	Particle- Particle	Particle- Fiber
Coefficient of restitution	0.5	0.5
Coefficient of static friction	0.6	0.4
Coefficient of rolling friction	0.05	0.05
Parameters	Values	
Particle diameter (μm)	10	
Number of particle injected	1000	
Time step for CFD (s)	$5 \times e^{-7}$	
Time step for DEM (s)	$5 \times e^{-9}$	
Simulation time (s)	0.02	

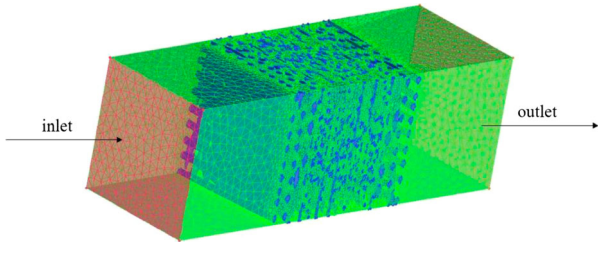

Figure 4. Mesh generation.

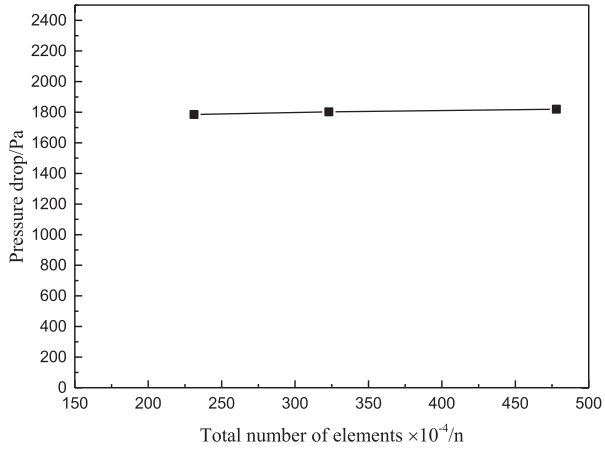

Figure 5. The effect of mesh density on the pressure drop.

3.4. Solution control

For transient calculation, it is required that the residuals in each time step are lower than the convergent residual standard. Monitored objects are continuity, x, y, z velocity, k and epsilon. The absolute criteria in this simulation is 10^{-4} and calculated residual in each time step is lower than it. Meanwhile, the mass flow rate of inlet and outlet are conservative. So the convergence of the numerical computation is achieved. Meanwhile, this simulation is computed by the computer with Intel® Xeon® CPU E5-2640 0 @ 2.50 GHz and 16 GB of memory. And the simulation time is about 3 weeks. Besides, the system used for this work is Windows 10.

4. Results and discussion

4.1. Particle filtration process

Figure 6 shows the movement of a spherical particle group at different times. The particle diameter of the coal particles is 10 μm. Driven by the inlet airstream, coal particles bypass the metal fibers and enter the inside of metal fiber felt through mesh channels. Gradually, more and more particles are intercepted by metal fibers, while a small portion of coal particles pass through the entire metal fiber felt model. The reasons are as follows. Firstly, the filtration process of metal fiber felt can be divided into two steps. The first step is steady filtration stage, in which particles are trapped due to the contact with fibers. And the following step is dynamic filtration stage, in which particles are trapped by dust layers formed on the surface of fibers. So as time goes on, the porosity of the metal fiber felt is reduced gradually. Therefore, more and more particles are intercepted by it. Secondly, the mesh channels formed by staggered fibers are of different sizes and no fixed shapes. So a small portion of particles can pass

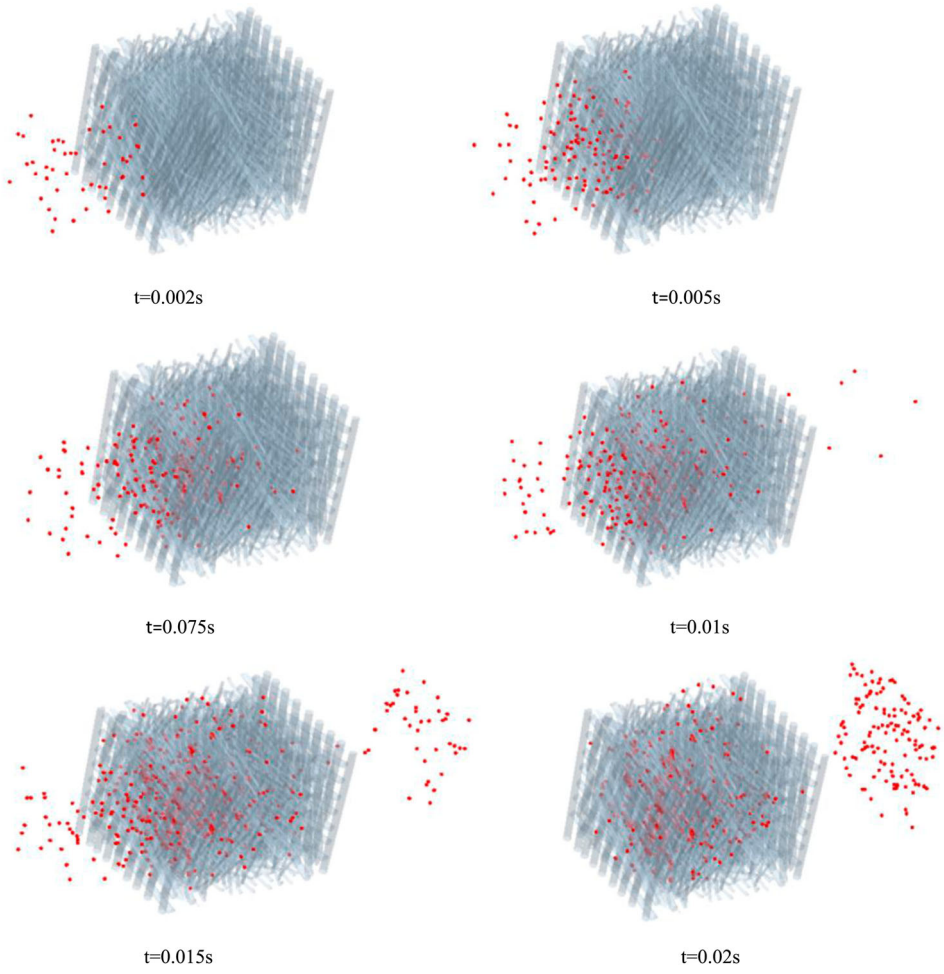

Figure 6. Changes of particle filtration process over time.

through the entire metal fiber felt by way of the larger mesh channels and avoid being intercepted. Meanwhile, the filtration of particles by fiber felt is mainly the result of diffusion effect, interception effect, deposition effect, inertial collision, and so on. When the particle size in airflow is less than 1 μm, especially less than 0.2 μm, particle will be under the movement of Brownian diffusion after the collision between particle and gas molecule (Kang, Lee, Kim, Chen, & Pui, 2019). But the particle size in the simulation is 10 μm, which is larger than the standard size. So diffusion effect didn't take lead effect in the study.

Two particles are randomly selected to study. One is intercepted by the metal fiber felt model and the other is a particle that passes through the entire metal fiber felt model. The trajectories of the two particles are shown in Figure 7(a,b) respectively. It can be seen from Figure 7 that the motion trajectory of the two particles in the metal fiber felt model is similar to a broken line before it stops. During the whole movement, particles collide with the metal fibers continuously when they are moving forward. And under the action of inlet airflow, particles bypass larger mesh channels with the motion of collision, rebound, refraction and so on.

4.2. Particle deposition distribution

As shown in Figure 8, the felt is equally divided into 20 regions along the thickness direction of the metal fiber felt model. Figure 9 shows the amount of particles deposited along the thickness direction of the metal fiber felt model at the end of the filtration process. As we can see from Figure 9, the deposition mode of particles exhibits a non-uniform distribution. The thickness of the region composed of 20 μm metal fibers is 0.1 mm. Although this is the first area to contact particles, there are only 72 particles intercepted. The reason for this is that the mesh channels formed by metal fibers in this area are larger than the volume of particles. The region composed of 8 μm metal fibers accounts for 0.296 mm and 772 particles are intercepted in this area, accounting for 90% of the intercepted particles. Therefore, the filter area formed by 8 μm metal fibers is the main area for the filter felt to capture particles. And the majority of particles are

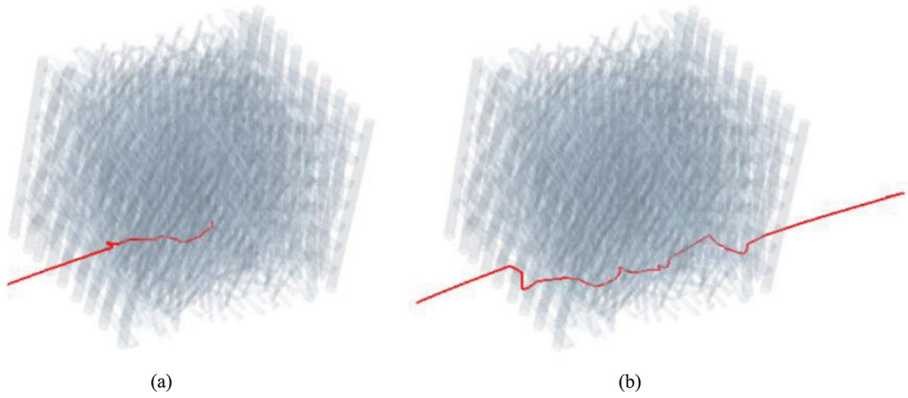

Figure 7. Particle trajectories. (a) Particle intercepted by the metal fiber felt model (b) Particle passing through the entire metal fiber felt model.

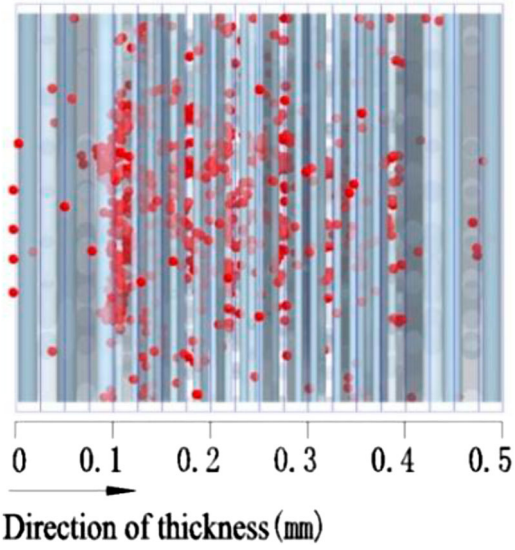

Figure 8. Blocks of metal fiber felt model.

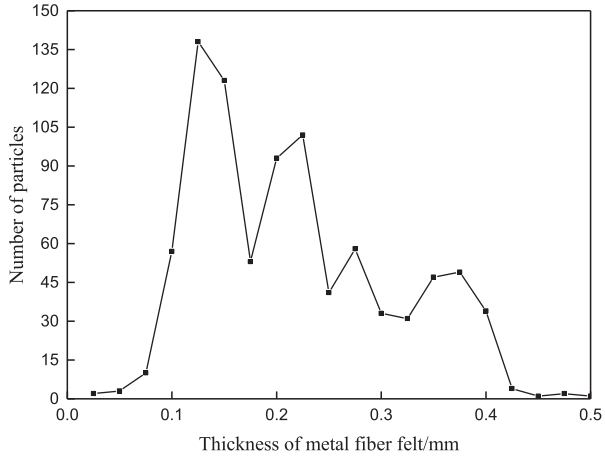

Figure 9. Number of deposited particles.

trapped due to the deep filtration of metal fiber felt. Particles intercepted in the middle region also show a non-uniform distribution and the number of them decreases along the thickness of felt gradually, which is consistent with the results of other literature (Riefler et al., 2018). The reason is that in the process of continuous collisions of particles with metal fibers, more and more particles are intercepted by the metal fibers ahead. So the number of particles that can be intercepted by the later metal fibers is also gradually reduced.

Figure 10 shows the deposition of particles at different positions inside the metal fiber felt model. The area where particles are densely deposited is mainly composed of two parts. One part is the intersection area formed by fibers with the diameter of 20 and 8 μm, as shown in Figure 10(a,b). And the other part is the area where smaller mesh channels are formed by metal fibers of 8 μm, which is shown in Figure 10(c,d).

The metal fiber felt model is made up of three regions. The outer two regions are composed of metal fibers with a diameter of 20 μm. The middle area is made up of metal fibers with a diameter of 8 μm. And the mesh channels formed by metal fibers of 20 μm in the outside region are relatively larger. So a large number of particles can continue to pass through the larger mesh channels. But when they move to the intersection area formed by fibers with the diameter of 20 and 8 μm, a part of the particles are intercepted because the space of the small mesh channels is smaller than particle volume. Besides, particles ahead bounce back because of the collision with 8 μm metal fibers. And the rebounding particles also collide with the particles moving forward. The kinetic energy is then sharply lost, and a large number of particles deposit at the intersection area. The following particles are intercepted under the joint action of the metal fibers and particles which are intercepted in front. Thus the space of the mesh channels is getting smaller and smaller. So a large number of particles are deposited in the intersection area formed by fibers with the diameter of 20 and 8 μm.

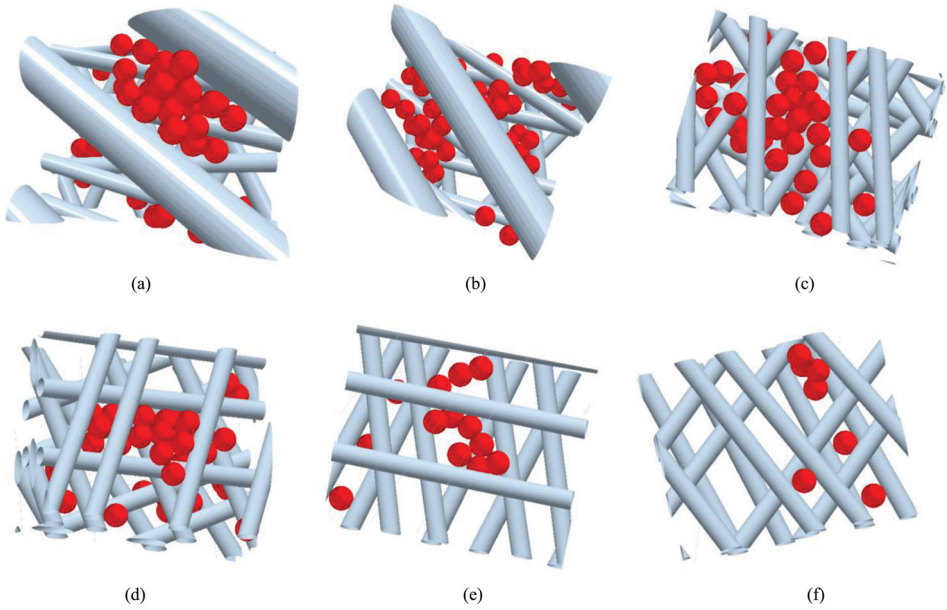

Figure 10. Deposition of particles in different positions. (a) $T = 0.125$ mm, (b) $T = 0.15$ mm, (c) $T = 0.2$ mm, (d) $T = 0.225$ mm, (e) $T = 0.3$ mm, (f) $T = 0.375$ mm.

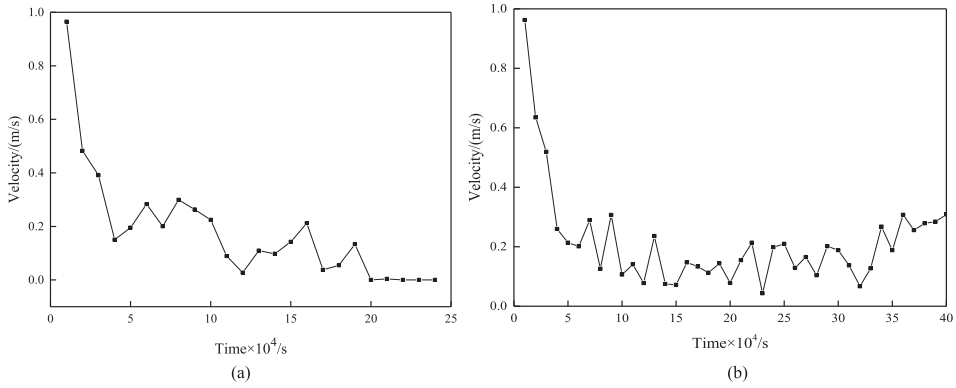

Figure 11. Distribution of particle velocity. (a) Particle intercepted by the metal fiber felt model, (b) Particle passing through the entire metal fiber felt model.

The particles that are not intercepted in the intersection area formed by fibers with the diameter of 20 and 8 μm continue to move by larger mesh channels. When particles arrive at the area with fine fibers, they are intercepted because the space is smaller than the volume of particles. A large number of particles in the back are intercepted by the interaction of metal fibers and intercepted particles in the front. So a lot of particles are intercepted in the area with smaller mesh channels.

Finally, it can be seen that there are two reasons for the interception of particles. On the one hand, the space of mesh channels formed by metal fibers is smaller than the volume of particles. It is not enough to keep particles passing through the metal fiber felt successfully. On the other hand, particles which are intercepted ahead reduce the space of the mesh channels. So under the joint action of the metal fibers and particles which are intercepted in front, the following particles are intercepted.

4.3. Analysis of particle velocity and kinetic energy

Two particles are randomly selected to study the change of velocity when they go through the whole metal fiber felt model. One is intercepted by the metal fiber felt model and the other is a particle that passes through the entire metal fiber felt model. The velocity changes are shown in Figure 11(a,b). We can see that particles travel at the speed of 1 m/s under the action of the airflow before coming into contact with the metal fiber felt model. Then, the velocity sharply decreases when particles collide with metal fibers. Driven by the inlet airflow, particles continue to move inside the metal fiber felt model, and

collide with metal fibers in the next layer. Then the particle velocity keeps dropping. After colliding with the multilayered metal fibers, particle velocity is maintained within the range of 0.15 to 0.25 m/s. Particles travel at a relatively stable speed in the area which is made up of 8 μm metal fibers. Finally, most particles are intercepted and remain stationary, while a few particles pass through the entire metal fiber felt model by larger mesh channels.

Figure 12 shows the change of kinetic energy loss caused by the collision of particles with the metal fiber felt. Two particles are selected. One is intercepted by the metal fiber felt model and the other is a particle that passes through the entire metal fiber felt model. As we could see from it, kinetic energy loss is sharply dropped in the period of 5×10^{-4} s, while the total time of the simulation is 0.02 s. So it can be clearly found that most of the kinetic energy loss occurs in the initial stage when particles pass through metal fiber felt. Especially, when particles collide with metal fibers for the first time, the kinetic energy loss is about 7 times larger than that of later collisions. The kinetic energy loss of particles tends to be stable with the movement of particles, which is basically maintained at 1×10^{-13} J. The reason is that particles slowly keep moving through mesh channels and the velocity maintains stable.

4.4. Experiment to verify the reliability of simulation method

In the realistic production, it's impossible to make each particle with the dimeter of 10 μm. So to verify the reliability of simulation method and model, we take some coal ash from the factory. Then, we use Mastersizer 2000 (Malvern Instrument) to analyze its particle size distribution, which is shown in Figure 13.

According to the results from the Mastersizer 2000, the size of particle is set to be normal distribution with the D50 of 12.420 μm in DEM and the Standard Deviation is 2.66. The filtration model of this case is shown in Figure 14. And the dust content of the gas is 254 g/m^3 in the simulation, which is consistent with the realistic dust gas. The air velocity inlet is set to be 1 m/s in it. Besides, the pressure drop of the coal ash from the factory is calculated to be 2024 Pa in the simulation.

Meanwhile, we do experiment with this actual dusty gas, whose dust content is 254 g/m^3. And the velocity of the dusty gas is 1 m/s with the density and viscosity values of 1.185 kg/m^3 and 1.834×10^{-5} Pa s. The experimental platform schematic is shown in Figure 15. Moreover, experimental platform is established as Figure 16. And pressure drop is measured as 2210 Pa in the experiment. As we can see, the result is a little larger than the

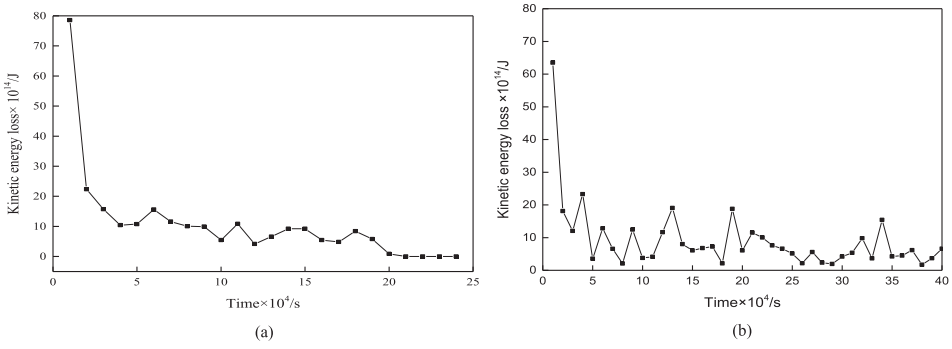

Figure 12. Kinetic energy loss of particles. (a) Particle intercepted by the metal fiber felt model, (b) Particle passing through the entire metal fiber felt model.

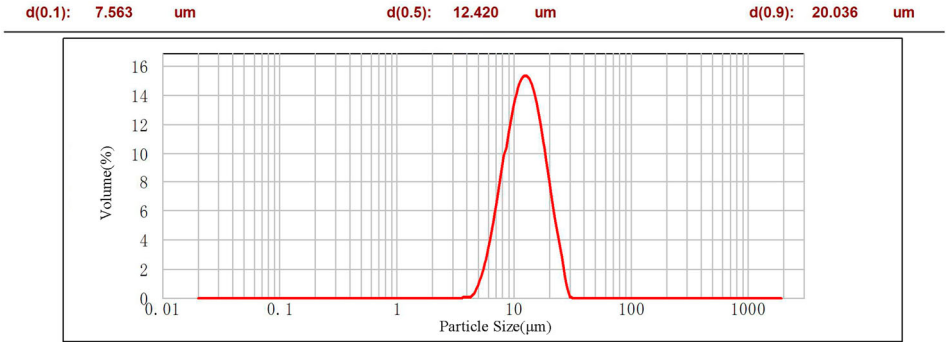

Figure 13. Particle size distribution.

Figure 14. Simulation of the coal ash from the factory. 1-Oil-free screw air compressor; 2-Ball valve; 3-Gas tank; 4-Control cabinet; 5-Turbine flowmeter; 6-Powder mixer; 7-Meta fiber felt; 8-Pressure gauge.

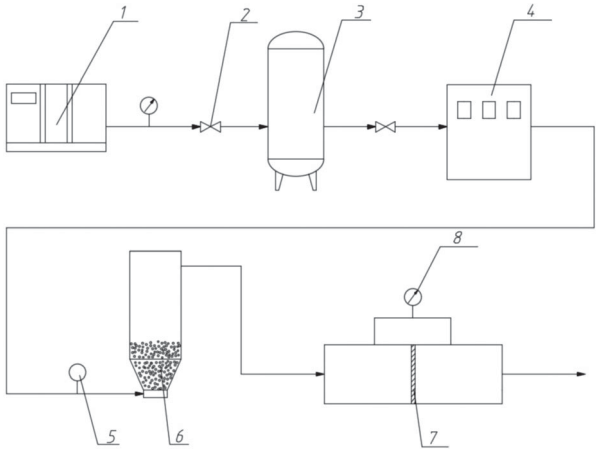

Figure 15. Experimental platform schematic.

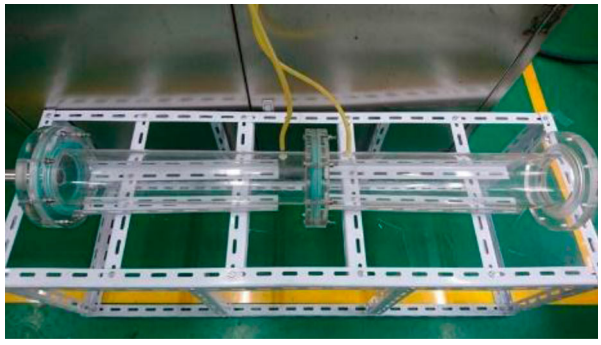

Figure 16. Experimental platform.

simulation. Because in the production process of metal fiber felt, there is a certain deformation in it, which is not a complete straight line of the fiber. So the result has a certain influence. Thus, we can conclude that the simulation method of the study is reliable.

5. Conclusions

Based on the microscopic images of the metal fiber felt obtained by scanning electron microscope, a three-dimensional model of the metal fiber felt is established. The CFD-DEM coupling simulation method is used to study the filtration process of spherical coal particles in the metal fiber felt. The simulation mainly studies moving trail and deposition characteristics of spherical coal particles at different positions. Conclusions are as follows:

(1) Driven by the airflow, coal particles bypass the metal fibers and enter the inside of the metal fiber felt through larger mesh channels. Moving trail of coal particles is similar to a broken line.
(2) Most coal particles are trapped due to the deep filtration of metal fiber felt and the distribution mode of coal particles is inhomogeneous. The number of particles trapped by metal fiber felt is gradually reduced in the direction of thickness.
(3) Coal particles are trapped not only by metal fibers randomly arranged on different layers of the metal fiber filter, but also by coal particles deposited previously.
(4) The kinetic energy loss of coal particles mainly occurs in the initial stage when particles pass through metal fiber felt. And the velocity of coal particles inside metal fiber felt is maintained at 0.15–0.25 m/s.

Further work on metal fiber felt will focus on the optimum matching relationship between operating conditions of dusty gas and metal fiber felt, which can be applied in industrial production to improve the production capacity and save resources. Moreover, one limitation of this study is that fibers in the model are straight, while actual material studied in this paper has some deformation during the molding process. This is what needs to be improved in the future.

Disclosure statement

No potential conflict of interest was reported by the authors.

Funding

This work was supported by Key Research and Development Plan of China Petrochemical Corporation (Sinopec Group) [grant number 418020-4].

References

Blais, B., Bertrand, O., Fradette, L., & Bertrand, F. (2017). CFD-DEM simulations of early turbulent solid-liquid mixing: Prediction of suspension curve and just-suspended speed. *Chemical Engineering Research and Design*, *123*, 388–406.

Buetehorn, S., Volmering, D., Vossenkaul, K., Wintgens, T., Wessling, M., & Melin, T. (2011). CFD simulation of single- and multi-phase flows through submerged membrane units with irregular fiber arrangement. *Journal of Membrane Science*, *384*(1–2), 184–197.

Cai, R., Zhang, L., & Bao, A. (2018). PM collection performance of electret filters electrospun with different dielectric materials-a numerical modeling and experimental study. *Building and Environment*, *131*, 210–219.

Cundall, P. A., & Strack, O. D. (1979). A discrete numerical model for granular assemblies. *Geotechnique*, *29*, 47–65.

Dong, L. (2016). The filtering accuracy of sintered metal porous materials. *Journal of Filtration & Separation*, *26*(2), 31–36. (in Chinese).

Dong, M., Li, J., Shang, Y., & Li, S. (2019). Numerical investigation on deposition process of submicron particles in collision with a single cylindrical fiber. *Journal of Aerosol Science*, *129*, 1–15.

Dong, K. J., Zou, R. P., Yang, R. Y., Yu, A. B., & Roach, G. (2009). DEM simulation of cake formation in sedimentation and filtration. *Minerals Engineering*, *22*(11), 921–930.

Gao, X., Li, T., Sarkar, A., Lu, L., & Rogers, W. A. (2018). Development and validation of an enhanced filtered drag model for simulating gas-solid fluidization of Geldart A particles in all flow regimes. *Chemical Engineering Science*, *184*, 33–51.

Hosseini, S. A., & Vahedi Tafreshi, H. (2012). Modeling particle-loaded single fiber efficiency and fiber drag using ANSYS-Fluent CFD code. *Computers & Fluids*, *66*, 157–166.

Kang, S., Lee, H., Kim, S. C., Chen, D., & Pui, D. Y. H. (2019). Modeling of fibrous filter media for ultrafine particle filtration. *Separation and Purification Technology*, *209*, 461–469.

Kaya, R., Deveci, G., Turken, T., Sengur, R., Guclu, S., Koseoglu-Imer, D. Y., & Koyuncu, I. (2014). Analysis of wall shear stress on the outside-in type hollow fiber membrane modules by CFD simulation. *Desalination*, *351*, 109–119.

Li, Y., & Ji, W. (2013). Acceleration of coupled granular flow and fluid flow simulations in pebble bed energy systems. *Nuclear Engineering and Design*, *258*, 275–283.

Li, W., Shen, S., & Li, H. (2016). Study and optimization of the filtration performance of multi-fiber filter. *Advanced Powder Technology*, *27*(2), 638–645.

Liu, X., Su, J., Qian, Y., Cui, L., & Liu, X. (2018). Comparison of two-fluid and discrete particle modeling of gas-particle flows in micro fluidized beds. *Powder Technology*, *338*, 79–86.

Liu, W., Xu, J., & Liu, X. (2016). Numerical study on collision characteristics for non-spherical particles in venturi powder ejector. *Vacuum*, *131*, 285–292.

Ma, C., Liu, Y., Li, F., Shen, C., Huang, M., Wang, Z., ... S and, W. (2019). CFD simulations of fiber-fiber interaction in a hollow fiber membrane bundle: Fiber distance and position matters. *Separation and Purification Technology*, *209*, 707–713.

Ma, L., Wei, L., Pei, X., Zhu, X., & Xu, D. (2018). CFD-DEM simulations of particle separation characteristic in centrifugal compounding force field. *Powder Technology*, *343*, 11–18.

Mahmoodi, B., Hosseini, S. H., & Ahmadi, G. (2018). CFD-DEM simulation of a pseudo-two-dimensional spouted bed comprising coarse particles. *Particuology*, *43*,171–180.

Mao, C., Lu, J., Zhao, Z., Yin, L., Hu, Y., & Bi, Z. (2017). Simulation and experiment of cutting characteristics for single cBN-WC-10Co fiber. *Precision Engineering*, *52*, 170–182.

Mou, B., He, B. J., Zhao, D. X., & Chau, K. W. (2017). Numerical simulation of the effects of building dimensional variation on wind pressure distribution. *Engineering Applications of Computational Fluid Mechanics*, *11*(1), 293–309.

Nakamura, K., Suda, T., & Matsumoto, K. (2018). Characterization of pore size distribution of non-woven fibrous filter by inscribed sphere within 3D filter model. *Separation & Purification Technology*, *197*, 289–294.

Qian, F., Huang, N., Lu, J., & Han, Y. (2014). CFD–DEM simulation of the filtration performance for fibrous media based on the mimic structure. *Computers and Chemical Engineering*, *71*, 478–488.

Qian, F., Huang, N., Zhu, X., & Lu, J. (2013). Numerical study of the gas-solid flow characteristic of fibrous media based on SEM using CFD-DEM. *Powder Technology*, *249*, 63–70.

Ramezanizadeh, M., Nazari, M. A., Ahmadi, M. H., & Chau, K. W. (2019). Experimental and numerical analysis of a nanofluidic thermosyphon heat exchanger. *Engineering Applications of Computational Fluid Mechanics*, *13*(1), 40–47.

Riefler, N., Ulrich, M., Morshäuser, M., & Fritsching, U. (2018). Particle penetration in fiber filters. *Particuology*, *40*, 70–79.

Saleh, A. M., Hosseini, S. A., Vahedi Tafreshi, H., & Pourdeyhimi, B. (2013). 3-D microscale simulation of dust-loading in thin flat-sheet filters: A comparison with 1-D macroscale simulations. *Chemical Engineering Science*, *99*, 284–291.

Saleh, A. M., & Vahedi Tafreshi, H. (2015). On the filtration performance of dust-loaded trilobal fibers. *Separation and Purification Technology*, *149*, 295–307.

Shi, Y., Matsunaga, T., Yamaguchi, Y., Li, Z., Gu, X., & Chen, X. (2018). Long-term trends and spatial patterns of satellite-retrieved $PM_{2.5}$ concentrations in South and Southeast Asia from 1999 to 2014. *Science of The Total Environment*, *615*, 177–186.

Sun, Z., Wen, J., Luo, X., Du, W., Liang, Z., & Fu, K. (2017). An improved CFD model of gas flow and particle interception in a fiber material. *Chinese Journal of Chemical Engineering*, *25*(3), 264–273.

Tian, W., Qi, L., Su, C., Zhou, J., & Jing, Z. (2016). Numerical simulation on elastic properties of short-fiber-reinforced metal matrix composites: Effect of fiber orientation. *Composite Structures*, *152*, 408–417.

Wu, H., Gui, N., Yang, X., Tu, J., & Jiang, S. (2017). Numerical simulation of heat transfer in packed pebble beds: CFD-DEM coupled with particle thermal radiation. *International Journal of Heat and Mass Transfer*, *110*, 393–405.

Wu, S. E., Lin, Y. C., Hwang, K. J., Cheng, T. W., & Tung, K. L. (2018). High-efficiency hollow fiber arrangement design to enhance filtration performance by CFD simulation. *Chemical Engineering & Processing Process Intensification*, *125*, 87–96.

Xu, J., Liu, X., & Pang, M. (2016). Numerical and experimental studies on transport properties of powder ejector based on double venturi effect. *Vacuum*, *134*, 92–98.

Yang, M., Li, S., & Yao, Q. (2013). Mechanistic studies of initial deposition of fine adhesive particles on a fiber using discrete-element methods. *Powder Technology*, *248*, 44–53.

Yue, C., Zhang, Q., & Zhai, Z. (2016). Numerical simulation of the filtration process in fibrous filters using CFD-DEM method. *Journal of Aerosol Science*, *101*, 174–187.

Zhuang, L., Guo, H., Dai, G., & Xu, Z. L. (2017). Effect of the inlet manifold on the performance of a hollow fiber membrane module-A CFD study. *Journal of Membrane Science*, *526*, 73–93.